Desalination and Water Treatment
www.deswater.com
doi: 10.5004/dwt.2020.24773

173 (2020) 243–254
January

Adsorption study of F^- ions onto ultrasonified electrochemically generated ultrafine particles

Kunjan Junghare, Shyam Kodape*, Virendra Jadhao

Department of Chemical Engineering, Visvesvaraya National Institute of Technology, Nagpur, Maharashtra, 440010, India, emails: samkodape@gmail.com (S. Kodape), kunjanjunghare@gmail.com (K. Junghare), virendra2j@gmail.com (V. Jadhao)

Received 26 March 2019; Accepted 8 August 2019

ABSTRACT

Ultrasonically improved electrochemically generated adsorbent (UEGA) has been synthesized and used for adsorption of fluoride ions from given aqueous solution. It is a two-step process, in the first step electrochemically generated adsorbent (EGA) has been prepared using electrolytic method and same was ultrasonicated to prepare UEGA. Ultrasonication causes an increase in adsorption by an increase in surface area which helps to enhance the defluoridation from the aqueous solution on the adsorbent. The kinetic models, adsorption isotherms and thermodynamic parameters such as enthalpy change $\Delta H°$, entropy change $\Delta S°$ and change in Gibbs free energy $\Delta G°$ have been analyzed during the adsorption process. Adsorption kinetic follows the pseudo-second-order model with highest correlation coefficient value, that is, 0.93. Furthermore, Temkin isotherm suggests the energy of adsorption 1.049 kJ/mol at operating temperature of 298 K. Characterizations such as Fourier transform infrared spectroscopy, scanning electron microscopy, energy dispersive spectroscopy, X-ray diffraction and specific surface analysis for Brunauer–Emmett–Teller has been performed to justify the mechanism and effect of ultrasonication on EGA. The overall study reveals that UEGA enhances defluoridation from aqueous solution.

Keywords: Ultrasonication; Defluoridation; Adsorption

1. Introduction

According to United States Geological Survey, only 2.5% fresh water is available on earth [1]. Out of these availabilities, there is fluoride contamination seen in the available groundwater [2,3]. There are many other contaminations but fluoride is brought into concern because of the worst impact it has on mankind. WHO in 1984 has prescribed a maximum tolerance limit of fluoride as 1.5 mg/L [4]. The Central Pollution Control Board, India standard allows 1.5 and 15 mg/L for drinking and industrially polluted wastewater, respectively [5]. Excessive consumption of fluoride can cause severe neuronal, skeletal and dental health problems [6]. Geographically major sources are found in the region characterized by inherent fluoride-rich metamorphic rocks such as leptynite, charnockite and khondalite [7,8]. In Maharashtra (India), Solapur, Karanja, Washim and states such as Punjab, Orissa and many other areas are affected by high fluoride content in groundwater as reported [9]. So fluoride removal for water purification has become a necessity whether it is drinking water, groundwater or industrial fluoride contaminated wastewater. Worldwide treatment technologies include membrane technique such as reverse osmosis, dialysis, electro-dialysis nanofiltration [10], adsorption [11], activated carbon [12], microbial fuel cell [13], electrocoagulation [14–16] at both laboratory and industrial level. Most of the treatment technologies are physicochemical in nature. Adsorption is the most widely used, as it is the simplest among all, due to its financial viability, easy fabrication, adsorbent generation and on site application [17].

* Corresponding author.

Adsorbent used for fluoride removal include impregnated alumina [18,19], impregnated resin [20], nano alumina [21], eucalyptus bark ash [22], red mud [23], aluminium hydroxide [24], coated nanoparticles [25]. Barathi et al. [18] showed that using ultrasonic waves on electrochemically generated adsorbents, which is a metal oxide, enhances its ability for electro-negative ions removal from the aqueous solution. Ultrasonic waves speed up the process of adsorption by increasing the surface area. There is a possibility of chelation between the electrochemically generated adsorbent and charged ions, which is fluoride in our case [26].

Our aim is to study the effect of ultrasonication on the electrochemically generated adsorbent in an attempt to increase its defluoridation capacity. Adsorbent preparation is carried out in two steps, first synthesis of electrochemically generated adsorbent (EGA) in an electrolytic reactor, second it is ultrasonicated in a sonicator to prepare ultrasonically improved electrochemically generated adsorbent (UEGA). Further, this adsorbent is exposed to ultrasonication to enhance fluoride removal efficiency. Literature proved that ultrasonication can enhance defluoridation by increasing the surface area [27]. Frequency of wave during the ultrasound is in the range 2×10^4 to 2×10^{10} Hz. When an ultrasonic wave is incident through a liquid medium, a large number of microbubbles originates, arise and collapse in a very short duration about a few microseconds called ultrasonic cavitations, which all results in a reduction of the surface area [28]. Since the ultrasonic frequency is used, leading to the process also being known as ultrasonication.

The mechanism of UEGA electrolytic method preparation is very similar to coagulant formation in chemical coagulation and electrocoagulation [29]. In the electrolytic method, the coagulant is produced in a controlled environment from electrochemical dissociation of a sacrificial anode. When current is supplied, trivalent metal hydroxide flocs are formed, depending upon which sacrificial anode was used. These metal hydroxide coagulant species have an affinity for fluoride ion removal.

The reaction occurring in the electrolytic reactor when aluminum acts as a sacrificial anode can be represented as follows [16]:

Anode:

$$Al_{(s)} \rightarrow Al^{3+} + 3e^- \quad (1)$$

Cathode:

$$2H_2O + 2e^- \rightarrow H_{2(g)} + 2OH^- \quad (2)$$

Precipitation of F^- ions with coagulant species:

$$Al^{3+} + 3H_2O \rightarrow Al(OH)_{3(s)} + 3H^+ \quad (3)$$

$$Al(OH)_3 + xF^- \leftrightarrow Al(OH)_{3-x}F_x + xOH^- \quad (4)$$

Oulebsir et al. [30] have generated adsorbents along with regeneration using the electrochemical technique for defluoridation. During the electrolytic process, the mechanics show the release of gases such as hydrogen, chlorine, and others depending upon the electrolyte used [31]. Very few papers are recognized in which ultrasonication is used for the enhancement of the adsorption capacity of adsorbents [32,33]. Reviewing all this we can combine the electrolytic process, ultrasonication and adsorption for effective fluoride removal from aqueous solutions.

2. Experimental

2.1. Chemicals and reagents

Sodium fluoride (NaF) (Fisher Scientific, India), sodium chloride (NaCl) and sodium hydroxide pellets (NaOH) (Merck Life Science, Mumbai), fluoride adjustment buffer powder pillows (HACH, Germany) were obtained and used without further treatment and purification. A stock solution of NaF (1,000 mg/L) and NaCl (0.1 M) were prepared using distilled water. Further dilution has been made according to the requirement in defluoridation experimentation. All the synthesis and experimentations were carried out at room temperature.

2.2. Instrumentation

Ultrasonication treatment to adsorbent has been carried out using Labman probe sonicator (Model PRO-250, 25 kHz, 3 mm diameter) in a soundproof box. A digital variable DC power supply (Scientific, 0–10 A, 0–30 V) has been used as a direct current source. Detection of fluoride ion (mg/L) was done using IntelliCAL FLUORIDE probe (ISEF 121) ion selective electrode (HACH, US). A TISAB buffer pillow was added during the measurement of fluoride ion concentration to eliminate the interferences of other ions in the sample. Agitation was provided using magnetic stirrer (REMI). The X-ray diffraction (XRD; Panalytical X'Pert-PRO) spectra of EGA and UEGA have been analyzed in the range of 10 to 100 and 0.0170 step size. Fourier transform infrared spectroscopy (FTIR) (Thermo Scientific Nicolet iS5) was used to study spectra from the range 4,000–400 cm^{-1}. The physical and morphological analysis of EGA and UEGA before and after ultrasonication was examined by scanning electron microscope (SEM) JSM-6380A (JEOL, Japan). Surface Area Analyzer SMART SORB-93 (Smart Instruments, Maharashtra) was used for the verification of surface area of the prepared adsorbent using helium and nitrogen as a carrier.

2.3. Preparation of ultrasonically improved electrochemically generated adsorbent (UEGA)

UEGA was prepared in two steps, in first step EGA was prepared in an electrolytic reactor as shown in Fig. 1 (acrylic, cylindrical flat bottom, 90 mm ID, 22 mm height). EGA is a solid complex formed as a product of electrochemical process governed by Eq. (3). In second step, EGA obtained from the first step was ultrasonicated. The electrolytic reactor consists of four aluminium electrode plates of thickness 3 mm and effective functional surface area of 125 cm^2. A direct current (DC) power supply was connected to electrodes which were arranged in a monopolar fashion with an inter electrode distance of 0.5 cm. EGA was prepared using 0.1 M NaCl electrolytic solution. The reaction volume, batch run time

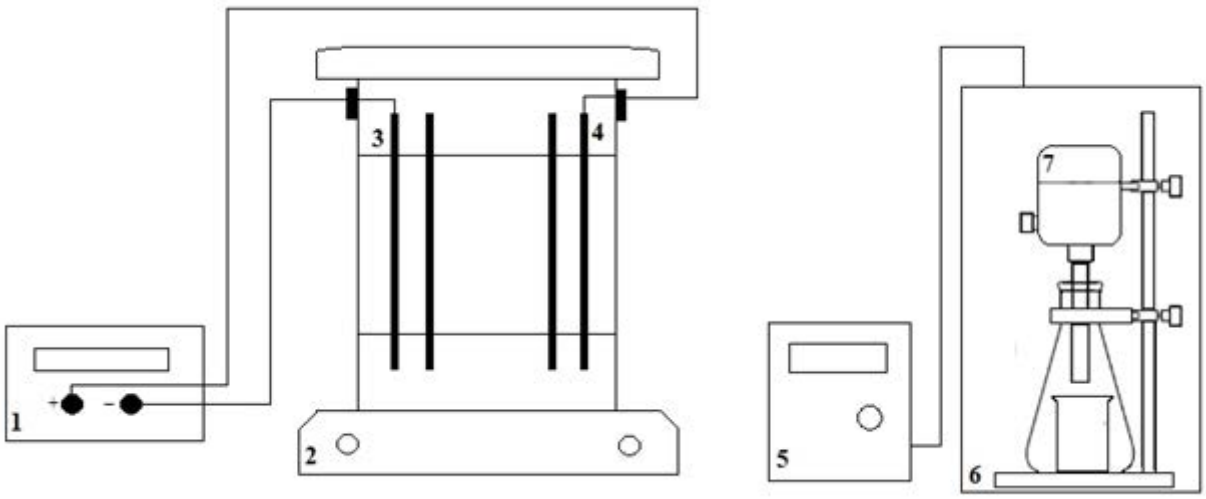

Fig. 1. Schematic representation of electrolytic reactor and probe sonicator where (1) electrolytic reactor; (2) magnetic stirrer; (3) cathode; (4) anode; (5) ultrasonic generator; (6) soundproof enclosure; (7) probe sonicator.

and current supplied were 1 L, 2 h and 1 A, respectively. Reactor content was well mixed using magnetic stirrer at the rate of 500 rpm. The sludge formed during the electrolytic process according to Eq. (3) was separated by gravity settling followed by filtration (Whatman 42 filter paper). The sludge was thermally treated at 80°C for 12 h hereafter it is called as EGA. In second step EGA and distilled water mixture was exposed to ultrasonication at 25 kHz amplitude for 15 min with 30 s pulse on and 5 s pulse off followed by separation using filtration and drying at 80°C for 12 h. Every time before commencement of step one, the electrode surface was cleaned by immersing in 0.1 M NaOH solution for 10 min followed by scrubbing using sandpaper to remove the passive layers [29] formed to avoid hindrance.

2.4. Batch defluoridation experiments

Batch experiments have been performed to study fluoride ion adsorption onto UEGA. A mixture of 0.2 g of UEGA and 40 mL NaF solution (10 mg/L) has been agitated for 15 min at 500 rpm and then left to rest till the equilibrium is reached. After fixed time interval, fluoride ion concentration left in the solution has been reported in terms of q_t as shown in Fig. 2. The amount of fluoride ion adsorbed onto UEGA at anytime t, q_t (mg/g) has been determined using Eq. (5) as follows:

$$q_t = \frac{C_0 - C_t}{W} \times V \tag{5}$$

where C_0 is initial fluoride concentration (mg/L) and C_t is fluoride ion concentration (mg/L) at anytime t, W is mass of UEGA material (gm) and V is volume of batch solution (mL). The amount of fluoride ion adsorbed per unit mass of adsorbent was calculated using Eq. (6)

$$q_e = \frac{C_0 - C_e}{W} \times V \tag{6}$$

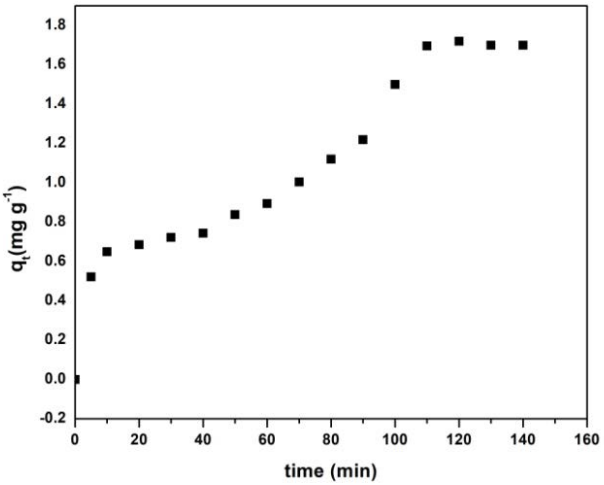

Fig. 2. q_t vs. time.

where q_e is the equilibrium adsorption capacity of fluoride ion on the adsorbent (mg/g), C_e is equilibrium fluoride concentration (mg/L) of fluoride ion in the aqueous solution.

2.5. Adsorption kinetics

The adsorption kinetics has been studied in order to verify mechanism, rate controlling step, rate of adsorption of fluoride ions using different kinetics models viz. pseudo-first-order model [34], pseudo-second-order model [35], intra-particle diffusion model [36], Elovich model, fractional power model [37] and Bhangham's model [38].

2.5.1. Pseudo-first-order model

The differential form of the pseudo-first-order mechanism is as follows:

$$\frac{dq}{dt} = k_1\left(q_t - q_e\right) \tag{7}$$

where k_1 is the rate constant for pseudo-first-order (min^{-1}) and t is time (min), integrating above equation at the boundary conditions $t = 0$ to $t = t$ and $q = 0$ to $q = q_t$ gives

$$\log(q_e - q_t) = \log q_e + \frac{k_1 t}{2.303} \tag{8}$$

A plot of $\log(q_e–q_t)$ vs. t gives the values of slope and intercept as $k_1/2.303$ and $\log q_e$, respectively.

2.5.2. Pseudo-second-order model

The differential form of the second order mechanism is as follows:

$$\frac{dq_t}{dt} = k_2(q_t - q_e)^2 \tag{9}$$

where k_2 is the rate constant for pseudo-second-order (g/mg min), integrating the above equation within the limits $t = 0$ to $t = t$ and $q = 0$ to $q = q_t$ which gives

$$\frac{t}{q_t} = \frac{1}{k_2 q_e^2} + \frac{t}{q_e} \tag{10}$$

A graph of t/q_t vs. t was plotted to obtain q_e and k_2.

2.5.3. Intra-particle diffusion model

This model was introduced by Weber and Morris. Its equation is stated below where k_3 is intra-particle diffusion model rate constant ($min^{-1/2}$) and C is the intercept (mg/g)

$$q_t = k_3 t^{0.5} + C \tag{11}$$

A plot q_t vs. $t^{0.5}$ will result a slope of k_3 and C

2.5.4. Elovich model

The Elovich model diffusion equation is given below, where α is initial adsorption rate (mg/g min) and β is the adsorption constant (g/mg).

$$q_t = \tfrac{1}{\beta}\ln(\alpha\beta) + \tfrac{1}{\beta}\ln t \tag{12}$$

By plotting a graph q_t vs. ln$t$, we get the value of α and β.

2.5.5. Fractional power model

The diffusion equation for fractional diffusion model is given as follows, where a and b are constants and $b < 1$

$$\log q_t = \log a + b\log t \tag{13}$$

Plotting the graph $\log q_t$ vs. log$t$, we get the constants a and b.

2.5.6. Bhangham's model

Bhangham's model diffusion equation is stated as

$$\log\left(\frac{C_0}{C_0 - q_t m}\right) = \log\left(\frac{k_0 m}{2.303V}\right) + \alpha\log t \tag{14}$$

where C_0 is initial concentration of adsorbate in solution (mg/L), m is weight of adsorbent per liter in solution (g/L) also α (<1) and k_0 are constants. Plot $\log\log\left(\frac{C_0}{C_{0-}q_t m}\right)$ vs. log$t$ we get the constants $k_{0.}$

2.6. Adsorption isotherms

Adsorption isotherm reveals the information about monolayer-multilayer, chemical–physical adsorption mechanism. It helps us to understand the interaction affinity between adsorbent and adsorbate. Four isotherm models have been studied viz. Langmuir isotherm [39], Freundlich isotherm, Dubinin–Radushkevich isotherm [40], Temkin isotherm [21]. The experiments have been carried out using a different initial concentration that is 10, 15 and 20 mg/L at room temperature.

2.6.1. Langmuir adsorption isotherm

Langmuir isotherm assumes uniform adsorbent surface and no interaction between adsorbate molecules, represented as equation below, where C_e is equilibrium concentration of fluoride ions (mg/L), q_0 is maximum adsorption capacity (mg/g), q_e is fluoride ions adsorbed at equilibrium condition (mg/g) and b is constant (mg/L) which signifies the energy of adsorption.

$$\frac{C_e}{q_e} = \frac{1}{q_0 b} + \frac{C_e}{q_0} \tag{15}$$

$$R_l = \frac{1}{1 + bC_0} \tag{16}$$

where R_L is a dimensionless parameter, Langmuir plot of C_e/q_e against C_e is graphed, q_0 and b values are obtained accordingly.

2.6.2. Freundlich isotherm

The aqueous solution is studied with this model and its equation is as follows

$$\log q_e = \log K_f + \frac{1}{n}\log C_e \tag{17}$$

where K_f is adsorption capacity (mg1–(1/n) L(1/n) g^{-1}) and n is intensity. A graph between $\log q_e$ and $\log C_e$ are plotted and K_f and n values are calculated.

2.6.3. Dubinin–Radushkevich isotherm

The Dubinin–Radushkevich isotherm equation is represented as follows:

$$\ln q_e = \ln q_m - \beta\varepsilon^2 \tag{18}$$

where q_m is the maximum capacity of adsorption and ε is Polanyi potential calculated using Eq. (19) as follows:

$$\varepsilon = RT\ln\left[1+\frac{1}{C_e}\right] \tag{19}$$

2.6.4. Temkin isotherm

The major assumptions of this model are there is uniform binding energy due to interactions between adsorbent–adsorbate and there is an inverse relationship between the heat of adsorption and surface coverage. The isotherm relationship is expressed below.

$$q_e = B_1 \ln K_T + B_1 \ln C_e \tag{20}$$

A plot of q_e vs. ln C_e was graphed to obtained B_1 and K_T, where $RT/b = B_1$, R is universal gas constant (8.314 J/mol K) and T is the temperature in Kelvin.

2.7. Thermodynamic study

Thermodynamic parameters such as enthalpy change $\Delta H°$ (J/mol) and entropy change $\Delta S°$ (J/mol) are related to change in Gibbs free energy $\Delta G°$ (J/mol). For the adsorption process, Gibbs free energy can be calculated using the equation as follows:

$$\Delta G° = -RT\ln K \tag{21}$$

where K is adsorption equilibrium constant, $\Delta H°$ and $\Delta S°$ are evaluated using Van't Hoff equation mentioned as follows:

$$\Delta G° = \Delta H° - T\Delta S° \tag{22}$$

This study helps to determine the favorable temperature for adsorption of fluoride ions onto UEGA material. The experiments were performed at three different temperatures 298, 308 and 313 K and the value of K was determined.

Combining Eqs. (21) and (22) gives

$$\ln K = \frac{-\Delta G°}{RT} = \frac{\Delta S°}{R} - \frac{\Delta H°}{RT} \tag{23}$$

where R is universal gas constant (8.314 J/mol K) and T is temperature (K). $\Delta H°$ and $\Delta S°$ values have been determined by plotting a graph of ln$K$ vs. 1/T

3. Results and discussion

3.1. Characterization of EGA and UEGA

3.1.1. XRD

The XRD analysis of the synthesized EGA and UEGA was carried out to determine the presence of crystalline and amorphous phases (Fig. 3). The intensity of peaks which is strong and sharp in EGA confirms crystalline nature as compared with UEGA which is characterized by medium mild signals. The reduction in the intensity of XRD spectra can be attributed as the effect of ultrasonication on EGA. It confirms that UEGA comprises of AlOOH and $Al(OH)_3$ through broad peaks at 2θ = 15° and 29° and same has been reported by Oulebsir et al. [30] and Zaidi et al. [43]. The existence of sodium aluminium oxide at 2θ = 18 [30] clearly specifies aluminium and aluminium complexes. Another characteristic strong sharp peak at 2θ = 41° was identified, indicating the presence of aluminium oxide. Other small peaks are identified which also confirmed the formation of aluminium compounds which also has a high affinity towards negatively charged fluoride ion and collectively taking part in defluoridation.

3.1.2. FTIR/EDS

The FTIR spectra (Fig. 4) of EGA and UEGA were examined in the diagnostic region and fingerprint region from their characteristic peak and respective wave numbers. In the

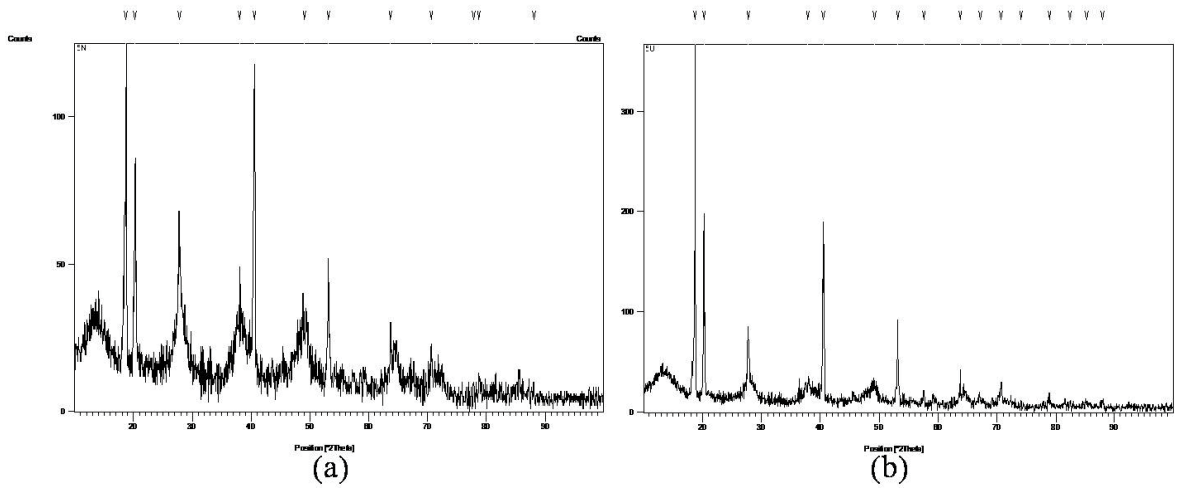

Fig. 3. XRD spectra of synthesized adsorbent (a) EGA and (b) UEGA.

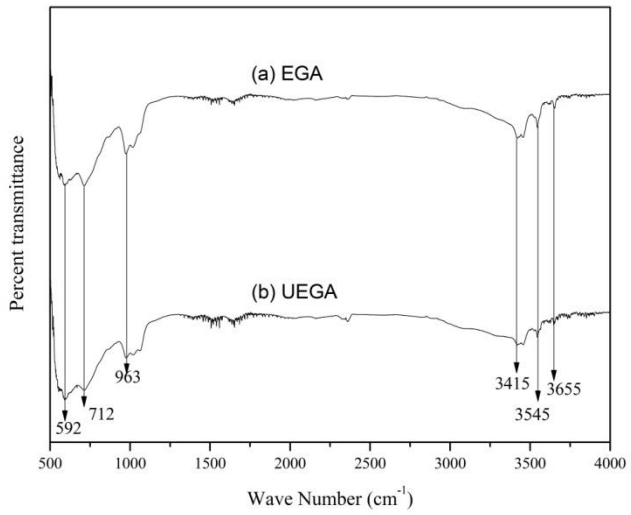

Fig. 4. FTIR spectra of synthesized adsorbent (a) EGA and (b) UEGA.

fingerprint region at 973 cm^{-1} can be attributed to Al–O–H band stretching with no hydrogen influence. The FTIR spectra of EGA show characteristic peaks between 550 and 963 cm^{-1} which confirms the presence of aluminium-oxygen (Al–O) stretching [11]. Confirmation of aluminium in pure form can be marked with a broad peak at 3,415 cm^{-1} [21], whereas vibrations at 3,000 and 3,600 cm^{-1} corresponds to aluminium hydroxide [30]. FTIR spectra of UEGA also show similar trends as that of EGA. Thus FTIR spectra confirmed that the adsorbent prepared as EGA and UEGA principally contained aluminium compounds and aluminium hydroxide complexes. The same elemental composition was corroborated using energy dispersive spectroscopy (EDS; Fig. 5). Furthermore, EDS examination of EGA and UEGA confirms Al and O were the principal elements observed. Presence of aluminium hydroxide complexes can also be seen undoubtedly in EDS which justifies its formation as represented in Eq. (4) as well as in FTIR. Traces of NaCl were noted, as it was used in the preparation of EGA and UEGA.

3.1.3. SEM

The morphology of unsonicated and sonicated adsorbents has been examined using SEM to study the effect of ultrasonication. Representative micrographs of EGA and UEGA were compared and shown in Fig. 6. EGA particles were found large in size with agglomerated bundles of sphere-like structure but not so well ordered in shape (Figs. 6a and c). On the other hand, UEGA are smaller not wholly spherical, but granular in shape and less agglomerated (Figs. 6b and d). The particle size of EGA obtained is 368 μm while for UEGA it ranges from 38 to 75 μm. Effect of ultrasonication is invincible as the reduction in particle size was visible using SEM characterization. Hence the formation of higher surface area which favored higher removal of fluoride by increasing the active sites available for adsorption [26], and the same behavior has been observed. Similarly, the percentage removal of fluoride ions by UEGA was comparatively faster than those by EGA, viz 93.5% and 78.9%, respectively (Fig. 7). Using BET surface area analyzer the reported surface area for UEGA is 73.13 m^2/mg. The effect of ultrasonication can be clearly seen in the micrographs, as there is a decrease in the particle size from EGA to UEGA. SEM micrographs of aluminium anode also show the increase in surface porosity before and after electrolytic method, thus it becoming highly microporous in structure as seen in Fig. 8.

3.2. Adsorption kinetics

The experimental data were obtained and were fitted in the kinetic models, the values of constants have been analyzed and summarized in Table 1. Experimental data for kinetic models are shown in Fig. 9. The best fit analysis was chosen on the basis of highest correlation co-efficient (R^2) and equilibrium capacity (q_e) values. The present

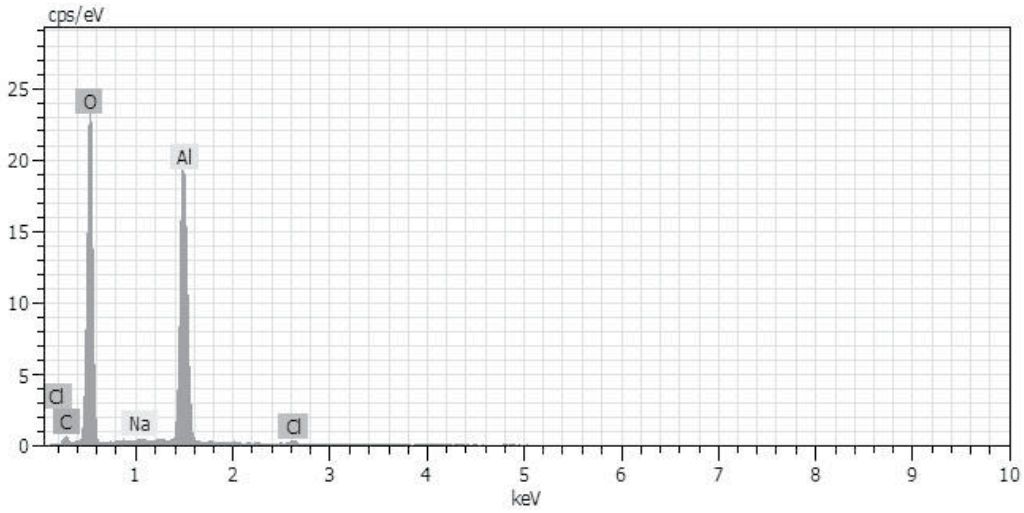

Fig. 5. EDS spectra of UEGA.

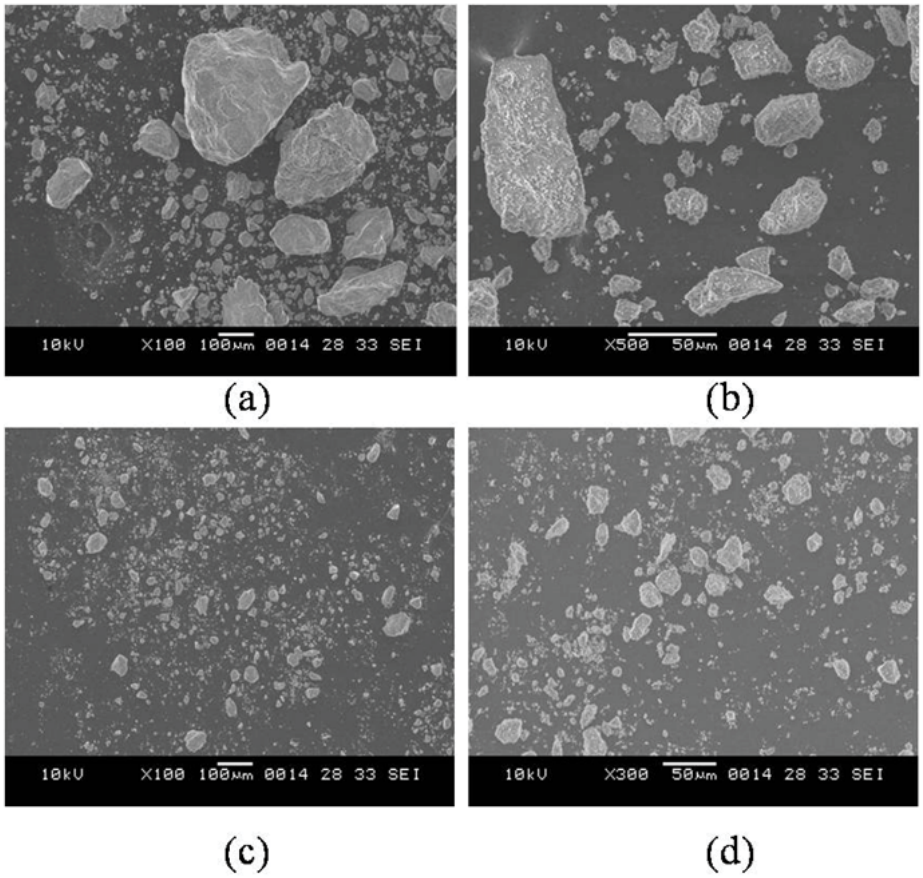

Fig. 6. SEM micrographs of synthesized adsorbent (a,b) EGA and (c,d) UEGA.

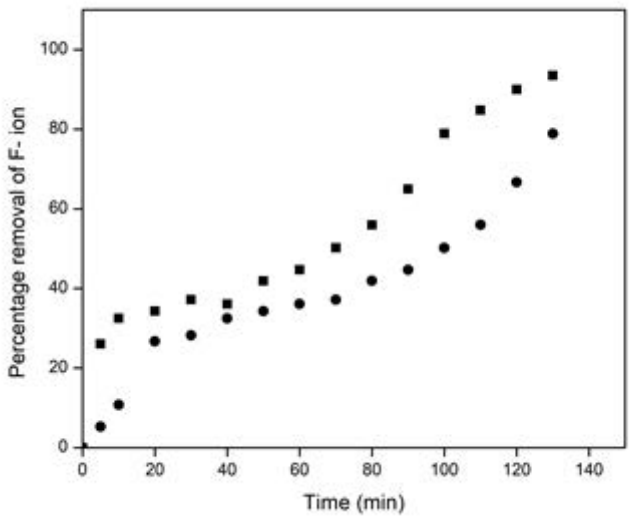

Fig. 7. Comparison between (●) EGA and (■) UEGA.

system follows pseudo-second-order kinetics as indicated by R^2 and q_e values that are 0.942 and 0.125, respectively, also the q_e values are close to experimental values. The R^2 values of other models such as the intra-particle diffusion model, pseudo-first-order model, fractional power model, Bhangham's model and elovich model are 0.914, 0.89, 0.873, 0.872 and 0.792, respectively. Pseudo-second-order kinetic model describes single-step chemisorptions as the rate determining step [40]. Hence we can conclude that the fluoride ion adsorption on UEGA material follows chemisorptions as R^2 values are closer to unity.

3.3. Adsorption isotherm

Graphical representations of different isotherm models viz. Langmuir adsorption isotherm, Freundlich isotherm, Dubinin–Radushkevich isotherm and Temkin isotherm are plotted in Fig. 10. Various parameters of these isotherms have been determined and tabulated in Table 2. The most promising model for this fluoride ion adsorption onto UEGA was found to be Temkin isotherm and the same has been validated by correlation coefficient, that is, 0.939. This model states that the heat of adsorption is inversely proportional to surface coverage because of adsorbent adsorbate interaction with consistent binding energy [21]. Value of b was found to be 1.049 kJ/mol which emphasize on electrostatic interaction between UEGA material and fluoride ions. The second best-fit isotherm model is Freundlich isotherm with its R^2 and K_T are 0.927 and 1.99. On the other hand, a poor correlation coefficient of Dubinin–Radushkevich and Langmuir isotherm are 0.911 and 0.799, respectively, proves them unfit for this study. It is also observed that the parameters such as q_m and β (i.e., 1.803 and 8×10^{-7}, respectively)

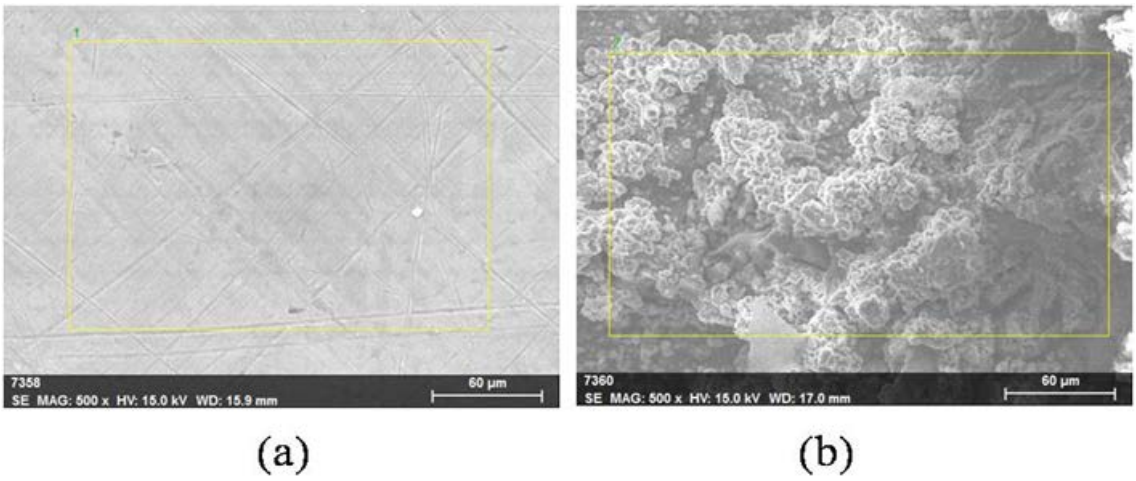

Fig. 8. SEM micrographs of sacrificial anode (a) before and (b) after.

Table 1
Kinetic parameters of models

Kinetic model	Adsorption parameters		R^2
Pseudo-first-order model	k_1 (min^{-1}) 6.909×10^{-3}	q_e (mg/g) 1.524	0.799
Pseudo-second-order model	k_2 (g/mg min) 7.466	q_e (mg/g) 0.1251	0.927
Intra-particle diffusion model	k_3 (g/mg min) 0.104	C 0.164	0.914
Elovich model	α 0.4607	β 4.8780	0.792
Fractional power model	a 0.33	b 0.257	0.873
Bhangham's model	α 0.259	k_0 (mL/gL) 1.322×10^3	0.872

of Dubinin–Radushkevich isotherm suggest exothermic interaction between fluoride ions and UEGA material [41]. The values of q_m and β were obtained graphically using a plot ln q_e vs. ε^2, which are 1.803 and 8×10^{-7}, respectively. The absorption energy (ε) liberated during this process is –790.56 J mol^{-1} which can be estimated using equation $\varepsilon = -(2\beta)^{-0.5}$ [40].

3.4. Adsorption thermodynamics

Thermodynamics helps us to find if the process is physical or chemical, spontaneous or non-spontaneous and endothermic or exothermic. It analyzes whether the adsorption process is affected by the change in temperature. All the thermodynamic parameters $\Delta G°$, $\Delta S°$ and $\Delta H°$ are listed in Table 3. The value of $\Delta H°$ and $\Delta S°$ were estimated using Eq. (22). $\Delta G°$ is found to be minimum at lowest temperature, that is, –5.645 kJ/mol using Eq. (21), hence the fluoride ion adsorption favors lower temperature [42], as it is exothermic process according to Le Chatelier's principle for any given pressure low temperatures are favored. Hence 298 K is found to be the optimum temperature for fluoride ion adsorption onto UEGA. The heat of reaction, $\Delta H°$ for the system was found to be negative, that is, –5.433 kJ/mol, hence heat is liberated and shows exothermic nature. The standard entropy $\Delta S°$ was also reported to be a negative indicating attraction between the fluoride ions and UEGA. Also $E_a = \Delta H° + RT$, where E_a is average activation energy which is found to be –51.85 kJ/mol. Thermodynamic parameters are tabulated in Table 2 and plots are shown in Fig. 11.

3.5. Comparison with aluminium adsorbent and regeneration of UEGA

UEGA is compared with other aluminum-based adsorbent. Minju et al. [25] reported that the particle size of the adsorbent is about 355 µm where as in this research, SEM indicates the particle size of 38–75 µm. On comparing the adsorption capacities from papers it ranges from 5 to 16 mg/g [30], 5–7 mg/g [25] and 7 mg/g for UEGA. The percentage removal efficiency is less by 4% since the initial fluoride concentration which is pretty high (15 mg/L) as compared with 5 mg/L [30].

Effective regeneration process covers factor such as percentage removal and number of batch experiments. In this study, synthesized UEGA was used up to four cycles for defluoridation. The reported percentage removal has been 93%, 91%, 89% and 82%. UEGA was regenerated using diluted sulfuric acid followed by filtration. Further multiple washing of adsorbent is attempted till neutral pH is observed followed by filtration and drying. This study on regeneration is attempted by Oulebsir et al. [30] and Du Du et al. [43] with a regeneration capacity of five and two cycles, respectively.

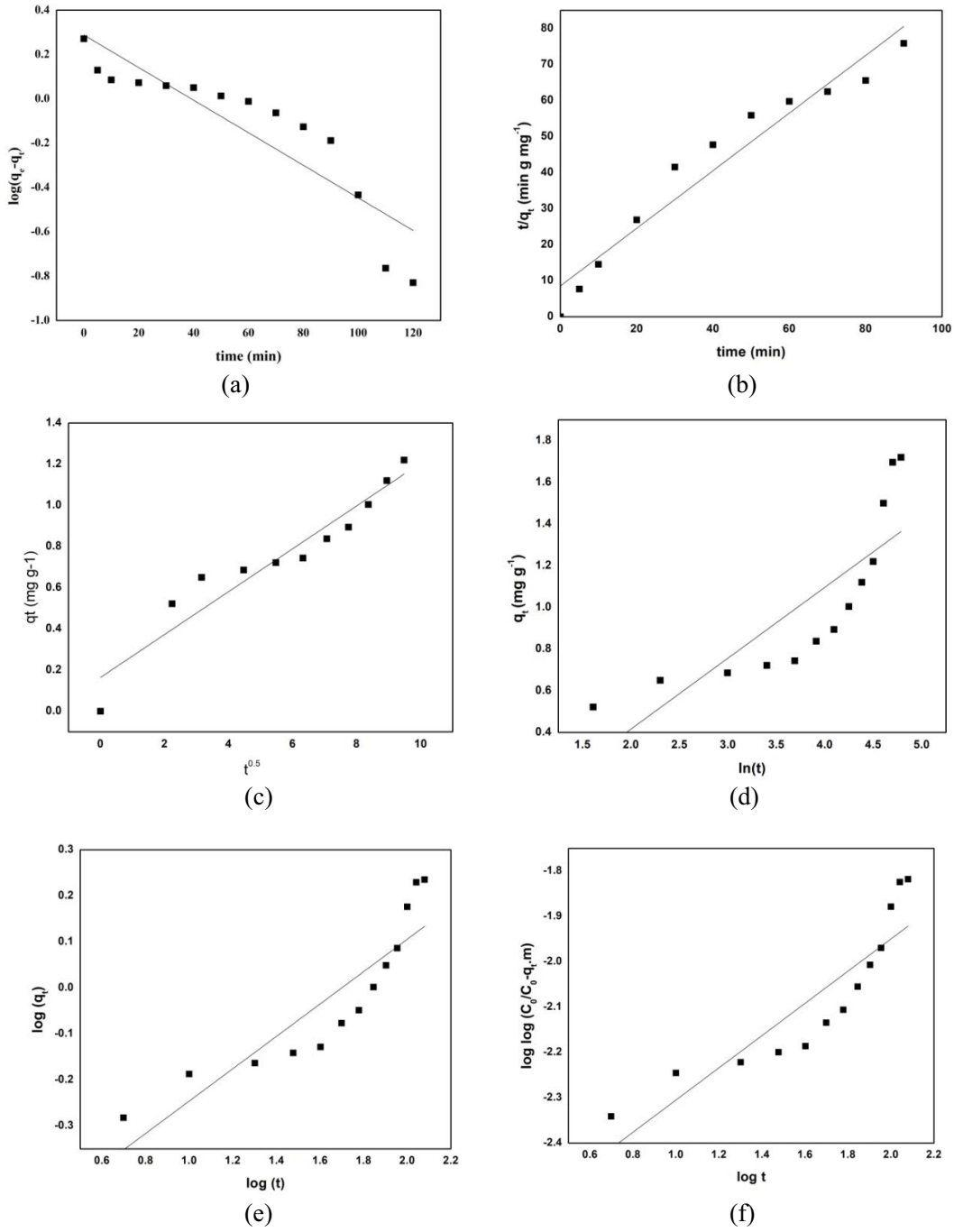

Fig. 9. Kinetic models: (a) pseudo-first-order, (b) pseudo-second-order, (c) intra-particle diffusion, (d) Elovich, (e) fractional power and (f) Bhangham.

Table 2
Adsorption isotherms for UEGA

Equilibrium isotherm	Parameters			R^2
Langmuir isotherm	b (L/mg) 0.374	q_0 (mg/g) 7.87	R_L 0.374	0.799
Freundlich	K_F (L/mg) 1.99		N 1.760	0.927
Dubinin–Radushkevich	β 8×10^{-7}	q_m 1.803		0.911
Temkin isotherm	K_T (L/mg) 1.724		B_1 2.377	0.939

Table 3
Thermodynamic parameters

Temperature (K)	$\Delta G°$ (kJ/mol)	$\Delta H°$ (kJ/mol)	$\Delta S°$ (kJ/mol)	E_a (kJ/mol)
298	–5.654			
308	–4.372	–54.331	–155.88	–51.85
313	–3.288			

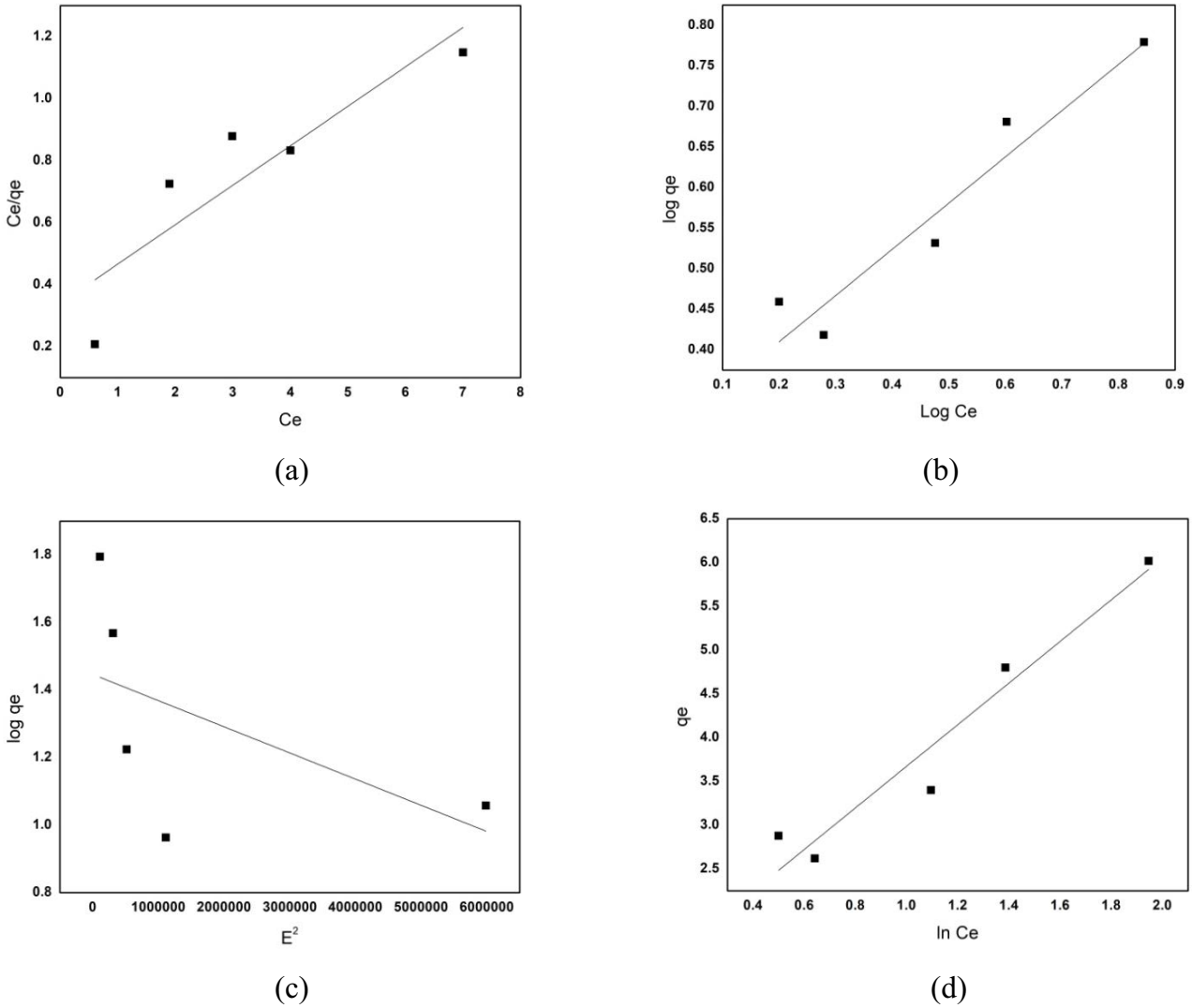

Fig. 10. Adsorption isotherms (a) Langmuir, (b) Freundlich, (c) Dubinin–Radushkevich and (d) Temkin isotherm.

4. Conclusion

UEGA was synthesized by electrolytic method followed by ultrasonication and was further characterized using SEM-EDS, FTIR, XRD, BET techniques. The outcome of this research proposes the enhancement in defluoridation by application of ultrasound on EGA causing effective particle size reduction. Significant size reduction of adsorbent from coarse particles (378 μm) to ultrafine particles (38–78 μm) has been examined. The percentage removal of fluoride ions by UEGA was comparatively faster than those by EGA, viz 93.5% and 78.9%, respectively. An XRD spectrum proves the existence of sodium aluminium oxide, aluminium and aluminium complexes, which further helps in defluoridation of wastewater. FTIR and EDS also confirmed that the adsorbent prepared as EGA and UEGA principally contained aluminium compounds and aluminium hydroxide complexes. SEM analysis shows that ultrasonication makes the adsorbent more small in particle size not wholly spherical but granular in shape and less agglomerated than EGA.

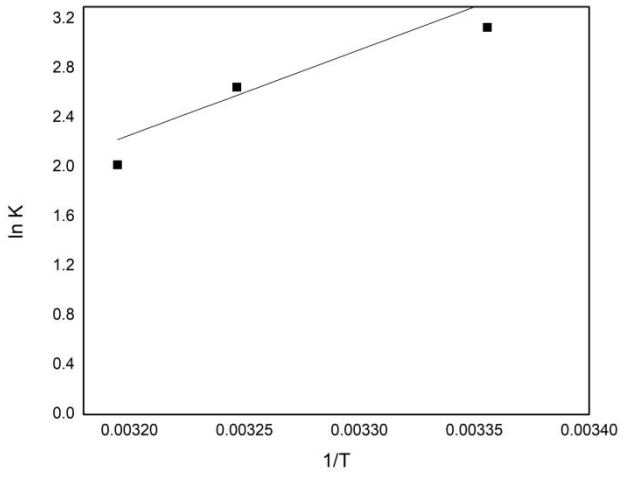

Fig. 11. Temperature effect on the adsorption of F^- ions onto UEGA particles.

XRD analysis confirms that UEGA comprises of AlOOH and $Al(OH)_3$ through broad peaks at 2θ = 15° and 29° and same has been reported by Oulebsir et al. [30] and Zaidi et al. [44]. Furthermore, EDS examination of EGA and UEGA confirms that Al and O were the principal elements observed. BET surface area analyzer declares the surface area of 73.13 m^2 associated with per gram of UEGA. Higher the surface area, it favors higher removal of fluoride by increasing the active sites available for adsorption. The adsorption kinetics of fluoride ions onto UEGA material follows pseudo-second-order kinetics which indicates single-step chemisorptions of fluoride as the rate determining step (R^2 = 0.927). Adsorption thermodynamics concludes that the process is exothermic in nature and favors lower temperature, that is, 298 K. Temkin isotherm is best-fitted isotherm for this adsorption study which suggests an inverse relationship between the heat of adsorption and surface covered with consistent binding energy. Similarly, thermodynamic parameters such as $\Delta H°$, $\Delta S°$ and E_a are found to be –54.331, –155.88 and –51.85 kJ/mol, respectively.

Acknowledgments

The author would like to thank and express gratitude to the Department of Chemical Engineering, Visvesvaraya National Institute of Technology, Nagpur, for providing well-equipped laboratories, their priceless assistance for characterization of adsorbent and carry out this research.

References

[1] P.H. Gleick, Water in Crisis: A Guide to the World's Fresh Water Resources, Oxford University Press, New York, 1993.
[2] G. Singh, B. Kumari, G. Sinam, N. Kumar, S. Mallick, Fluoride distribution and contamination in the water, soil and plants continuum and its remedial technologies, an Indian perspective – a review, Environ. Pollut., 239 (2018) 95–108.
[3] R. Thapa, S. Gupta, A. Gupta, D. Venkat, H. Kaur, Geochemical and geostatistical appraisal of fluoride contamination: an insight into the Quaternary aquifer, Sci. Total Environ., 640–641 (2018) 406–418.
[4] World Health Organization (WHO), Guidelines for Drinking-Water Quality: Incorporating First Addendum Recommendations, 3 (2006) 375–376.
[5] MoEF, The Environment (Protection) Rules. New Delhi: Ministry of Environment and Forest; 1986.
[6] S. Dey, B. Giri, Fluoride fact on human health and health problems: a review, iMedPub J., 2 (2016) 1–6.
[7] K. Brindha, L. Elango, Geochemistry of fluoride rich groundwater in a weathered Granitic rock region, southern India, Water Qual. Expo Health, 5 (2013) 127–138.
[8] S. Shekhar, A.C. Pandey, M.S. Nathawat, Evaluation of fluoride contamination in groundwater sources in hard rock terrain in Garhwa district, Jharkhand, India, Int. J. Environ. Sci., 3 (2012) 1022–1030.
[9] K. Brindha, R. Rajesh, R. Murugan, L. Elango, Fluoride contamination in groundwater in parts of Nalgonda District, Andhra Pradesh, India, Environ. Monit. Assess., 172 (2011) 481–492.
[10] Y. Zhang, C. Causserand, P. Aimar, J.P. Cravedi, Removal of bisphenol A by a nanofiltration membrane in view of drinking water production, Water Res., 40 (2006) 3793–3799.
[11] D. Mehta, P. Mondal, S. George, Utilization of marble waste powder as a novel adsorbent for removal of fluoride ions from aqueous solution, Biochem. Pharmacol., 4 (2016) 932–942.
[12] S. Roy, P. Das, S. Sengupta, S. Manna, Calcium impregnated activated charcoal: optimization and efficiency for the treatment of fluoride containing solution in batch and fixed bed reactor, Process Saf. Environ. Prot., 3 (2017) 265–277.
[13] A. Yewale, R. Methekar, S. Agrawal, Dynamic analysis and multiple model control of continuous microbial fuel cell (CMFC), Chem. Eng. Res. Des., 148 (2019) 403–416.
[14] M. Behbahani, M.R.A. Moghaddam, M. Arami, Techno-economical evaluation of fluoride removal by electrocoagulation process: optimization through response surface methodology, Desalination, 271 (2011) 209–218.
[15] J. Zhu, H. Zhao, J. Ni, Fluoride distribution in electrocoagulation defluoridation process, Sep. Purif. Technol., 56 (2007) 184–191.
[16] M.M. Emamjomeh, M. Sivakumar, A.S. Varyani, Analysis and the understanding of fluoride removal mechanisms by an electrocoagulation/flotation (ECF) process, Desalination, 275 (2011) 102–106.
[17] D.M. Ruthven, Principles of Adsorption and Adsorption Processes, Wiley, USA, 1984.
[18] M. Barathi, A.S.K. Kumar, N. Rajesh, A novel ultrasonication method in the preparation of zirconium impregnated cellulose for effective fluoride adsorption, Ultrason. Sonochem., 21 (2014) 1090–1099.
[19] S. Bibi, A. Farooqi, K. Hussain, N. Haider, Evaluation of industrial based adsorbents for simultaneous removal of arsenic and fluoride from drinking water, J. Clean. Prod., 87 (2015) 882–896.
[20] M. Barathi, A.S.K. Kumar, N. Rajesh, Aluminium hydroxide impregnated macroreticular aromatic polymeric resin as a sustainable option for defluoridation, J. Environ. Chem. Eng., 3 (2015) 630–641.
[21] P. Shivaprasad, P.K. Singh, V.K. Saharan, S. George, Synthesis of nano alumina for defluoridation of drinking water, Nano-Struct. Nano-Objects., 13 (2018) 109–120.
[22] S.B. Ghosh, N.K. Mondal, Application of Taguchi method for optimizing the process parameters for the removal of fluoride by Al-impregnated Eucalyptus bark ash, Environ. Nanotechnol., Monit. Manage., 11 (2019) 234–245.
[23] S. Zhu, D. Zhu, X. Wang, Removal of fluorine from red mud (bauxite residue) by electrokinetics, Electrochim. Acta, 242 (2017) 300–306.
[24] V.K. Jadhao, S. Kodape, K. Junghare, Optimization of electrocoagulation process for fluoride removal: a blending approach using gypsum plaster rich wastewater, Sustain. Environ. Res., 29 (2019) 1–9.
[25] N. Minju, K. Venkat Swaroop, K. Haribabu, V. Sivasubramanian, P. Senthil Kumar, Removal of fluoride from aqueous media by

magnesium oxide-coated nanoparticles, Desal. Wat. Treat., 53 (2015) 2905–2914.
[26] H. Zengin, G. Kalayci, G. Zengin, Effect of sonication in the preparation of activated carbon particles on adsorption performance effect of sonication in the preparation of activated carbon particles on adsorption performance, Sep. Sci. Technol., 49 (2014) 1807–1816.
[27] S. Sompech, A. Srion, A. Nuntiya, The effect of ultrasonic treatment on the particle size and specific surface area of LaCoO3, Procedia Eng., 32 (2012) 1012–1018.
[28] T.J. Mason, J.P. Lorimer, Theory, Applications and Uses of Ultrasound in Chemistry J.P., 2014.
[29] G. Mouedhen, M. Feki, M.D.P. Wery, H.F. Ayedi, Behavior of aluminum electrodes in electrocoagulation process, J. Hazard. Mater., 150 (2008) 124–135.
[30] A. Oulebsir, T. Chaabane, S. Zaidi, K. Omine, V. Alonzo, A. Darchen, T.A.M. Msagati, V. Shivasankar, Preparation of mesoporous alumina electro-generated by electrocoagulation in NaCl electrolyte and application in fluoride removal with consistent regenerations, Arab. J. Chem., 4 (2015) 234–266.
[31] M.A. Nasution, Z. Yaakob, E. Ali, N.B. Lan, S. Rozaimah, S. Abdullah, A comparative study using aluminum and iron electrodes for the electrocoagulation of palm oil mill effluent to reduce its polluting nature and hydrogen production simultaneously, Pakistan J. Zool., 45 (2013) 331–337.
[32] A. Deghles, U. Kurt, Hydrogen gas production from tannery wastewater by electrocoagulation of a continuous mode with simultaneous pollutants removal, IOSR J. Appl. Chem., 10 (2017) 40–50.
[33] A. Nasution, B.L. Ng, E. Ali, Z. Yaakob, S.K. Kamarudin, Electrocoagulation of palm oil mill effluent for treatment and hydrogen production using response surface methodology, Polish J. Environ. Stud., 23 (2014) 1669–1677.
[34] H. Moussout, H. Ahlafi, M. Aazza, H. Maghat, Critical of linear and nonlinear equations of pseudo-first order and pseudo-second order kinetic models, Karbala, Int. J. Mod. Sci., 4 (2018) 244–254.
[35] Y.S. Ho, G. Mckay, Pseudo-second order model for sorption processes, Process Biochem., 34 (1999) 451–465.
[36] Y.S. Ho, G. Mckay, T. Hong, W. Bay, H. Kong, T. Hong, Kinetics of pollutant sorption by biosorbents: Review, Sep. Purif. Rev., 2 (2013) 37–41.
[37] R.C. Dalal, Desorption of soil phosphate by anion-exchange resin, Commun. Soil Sci. Plant Anal., 5 (1974) 531–538.
[38] C. Aharoni, S. Sideman, E. Hoffer, Adsorption of phosphate ions by collodion-coated alumina, J. Chem. Technol. Biotechnol., 29 (1979) 404–412.
[39] Sivarajasekar, T. Paramasivan, S. Muthusaravanan, P. Muthukumaran, S. Sivamani, Defluoridation of water using adsorbents - a concise review, J. Environ. Pollut., 6 (2017) 186–198.
[40] S.S. Madan, K.L. Wasewar, C.R. Kumar, Adsorption kinetics, thermodynamics, and equilibrium of a -toluic acid onto calcium peroxide nanoparticles, Adv. Powder Technol., 3 (2016) 235–267.
[41] V.S. Mane, I. Deo Mall, V. Chandra Srivastava, Kinetic and equilibrium isotherm studies for the adsorptive removal of Brilliant Green dye from aqueous solution by rice husk ash, J. Environ. Manage., 84 (2007) 390–400.
[42] B. Meroufel, O. Benali, M. Benyahia, Y. Benmoussa, M.A. Zenasni, Adsorptive removal of anionic dye from aqueous solutions by mixture of Kaolin and Bentonite clay: characteristics, isotherm, kinetic and thermodynamic studies, Iran. J. Energy Environ., 6 (2015) 482–491.
[43] X. Du, J. Xue, X. Wang, Y. Chen, J. Ran, L. Zhang, Oxidation of sulfur dioxide over V_2O_5/TiO_2 catalyst with low vanadium loading: a theoretical study, J. Phys. Chem. C, 122 (2018) 4517–4523.
[44] S. Zaidi, T. Chaabane, T.A.M. Msagati, Electro-coagulation coupled electro-flotation process: feasible choice in doxycycline removal from pharmaceutical effluents, Arabian J. Chem., 23 (2015) 0–11.